

# Quarkonium dissociation in a far-from-equilibrium holographic setup

L. Bellantuono,<sup>1,2</sup> P. Colangelo,<sup>2</sup> F. De Fazio,<sup>2</sup> F. Giannuzzi,<sup>2</sup> and S. Nicotri<sup>2</sup>

<sup>1</sup>*Dipartimento Interateneo di Fisica “M. Merlin”, Università e Politecnico di Bari, Italy*

<sup>2</sup>*Istituto Nazionale di Fisica Nucleare, Sezione di Bari, Italy*

The real-time dissociation of the heavy quarkonium in a strongly coupled boost-invariant non-Abelian plasma relaxing towards equilibrium is analyzed in a holographic framework. The effects driving the plasma out of equilibrium are described by boundary quenching, impulsive variations of the boundary metric. Quarkonium is represented by a classical string with endpoints kept close to the boundary. The evolution of the string profile is computed in the time-dependent geometry, and the dissociation time is evaluated for different configurations with respect to the direction of the plasma expansion. Dissociation occurs quickly for the quarkonium placed in the transverse plane.

PACS numbers: 12.38.Mb, 11.25.Tq

The discovery that the QCD matter produced in ultrarelativistic heavy ion collisions behaves as a high-temperature, nearly frictionless, strongly coupled fluid raises new questions, both to experiment and theory [1]. On the one hand, through the study of new production modes and observables it is important to identify the smallest size of the QCD system characterized by this behavior, interpreting the hints of collective features observed in high energy  $pp$  and  $pA$  collisions [2]. On the other hand, the real-time dynamics of the relaxing fluid needs to be quantitatively described, starting from the far-from-equilibrium state produced immediately after the collision and relaxing towards a hydrodynamic regime: this issue is difficult to face using traditional theoretical techniques, which deal either with weakly coupled systems or, as in lattice QCD, with systems at equilibrium in the Euclidean time. The importance of theoretical analyses of processes occurring in out-of-equilibrium matter has been recently emphasized [3]. Among those phenomena, the heavy quarkonium dissociation plays a role in the characterization of the plasma, since it can be interpreted as a signature of deconfinement [4].

Gauge/gravity duality [5–7] (“holographic”) methods provide tools to describe out-of-equilibrium strongly coupled systems, mapping the dynamics of a gauge system into a gravity problem. Although the existence of a gravitational dual of QCD has not been established, yet, insights can be gained by the study of theories sharing various properties with QCD. In particular, a plasma of  $\mathcal{N} = 4$  supersymmetric Yang-Mills theory (SYM), similarly to the QCD plasma (QGP), is nonconfined and strongly interacting. Adopting the gauge/gravity approach the gravitational dual of  $\mathcal{N} = 4$  SYM in the large  $N_c$  limit, the ten dimensional  $AdS_5 \times S^5$  space, can be considered, with a black-hole (BH) to describe the boundary theory at finite temperature <sup>1</sup>.

In this framework, quarks can be treated as dual to open strings in the higher dimensional space [11]. Their in-medium dynamics is described starting from the initial configuration of a classical string in the dual space, and following the string evolution dictated by the equations of motion resulting from the Nambu-Goto action.

Different configurations have been considered in a static gravitational background. One consists in a string created at an initial time at a point in space, which evolves into an extended string falling down under the action of gravity, with the endpoints moving in opposite directions. In this way, the drag force experienced by a heavy quark traveling in a strongly coupled plasma [12, 13] and the diffusion coefficient have been evaluated [14–16]. At finite temperature the trajectories of the endpoints approach lightlike geodesics at early times [17, 18], and thermalization occurs when the BH horizon is reached. The largest penetration depth  $\Delta x$  reached by a quark with energy  $E$  before thermalizing turns out to be an increasing function of the energy: the scaling law  $\Delta x \propto E^{1/3}$  has been determined [19], and an analytical proof that the penetration depth for a light quark is bounded by the curve  $\Delta x = \text{const} \cdot E^{1/3}$  has been provided [18]. For light quarks, the energy loss has been found to be sensitive to the initial conditions, and a peak before thermalization has been observed, sometimes denoted as explosive burst of energy [18].

For a quarkonium moving in the plasma, the screening length has been evaluated by a Wilson loop computation [20–22], and the Wilson loop in the Vaidya geometry has also been examined [23]. Here, we look at the real-time evolution of a string stretched between two endpoints (representing the heavy quark and antiquark) kept close to the boundary. The string falls down under gravity and, at finite temperature, it can reach the BH horizon: this is interpreted as the quarkonium dissociation in the thermalized medium [24, 25].

<sup>1</sup> An introduction to gauge/gravity methods can be found in [8], and numerical approaches are discussed in [9]. Applications to the phenomenology of ultrarelativistic heavy ion collision are reviewed in [10].

To describe the dynamics in the out-of-equilibrium matter, we consider the time-dependent dual geometry obtained through a quench, a distortion of the boundary metric mimicking an impulsive effect which drives the boundary system far from equilibrium [26, 27]. We denote the  $4D$  boundary coordinates as  $x^\mu = (x^0, x^1, x^2, x^3)$ , with  $x^3 = x_\parallel$  the axis in the collision direction. We study the case where boost invariance along this axis is imposed, together with translation and  $O(2)$  rotational invariance in the  $x_\perp = \{x^1, x^2\}$  plane. In terms of the proper time  $t$  and of the spatial rapidity  $y$ , with  $x^0 = t \cosh y$ ,  $x_\parallel = t \sinh y$ , the  $4D$  line element is written as <sup>2</sup>:  $ds_4^2 = -dt^2 + dx_\perp^2 + t^2 dy^2$ . A quench is introduced as an anisotropic distortion of the boundary metric which leaves the spatial three-volume unchanged and maintains the other symmetries. The line element  $ds_4^2$  is modified as

$$ds_4^2 = -dt^2 + e^{\gamma(t)} dx_\perp^2 + t^2 e^{-2\gamma(t)} dy^2, \quad (1)$$

with quench profile  $\gamma(t)$ . Equation (1) can be considered as the boundary metric of the  $5D$  space where the gravity dual is defined. Using Eddington-Finkelstein coordinates, with  $r$  the fifth (holographic) coordinate, the  $5D$  bulk metric can be written as

$$ds_5^2 = 2drdt - Adt^2 + \Sigma^2 e^B dx_\perp^2 + \Sigma^2 e^{-2B} dy^2, \quad (2)$$

with the boundary obtained for  $r \rightarrow \infty$ . The metric functions  $A$ ,  $\Sigma$  and  $B$  only depend on  $r$  and  $t$ , due to the imposed symmetries. They are determined solving  $5D$  Einstein vacuum equations with negative cosmological constant, with two boundary conditions. The first one is that the metric (2) reproduces (1) for  $r \rightarrow \infty$ . Moreover, focusing on distortion profiles in a time interval  $[t_i, t_f]$ , the metric functions must correspond to  $\text{AdS}_5$  at  $t = t_i$  [27].

In [28, 29] several quench profiles have been investigated, describing sequences of pulses with different intensities and duration. Here we focus on two cases, one denoted as model  $\mathcal{A}(2)$ , consisting of two overlapping short pulses, and one as model  $\mathcal{B}$ , a smooth distortion with a pulse superimposed [28]. They are obtained choosing the profiles

$$\gamma(t) = w_\gamma \left[ \tanh \left( \frac{t - t_0}{\eta} \right) \right]^7 + \sum_{j=1}^N \gamma_j(t, t_{0,j}) \quad (3)$$

with

$$\gamma_j(t, t_{0,j}) = c_j f_j(t, t_{0,j})^6 e^{-1/f_j(t, t_{0,j})} \Theta \left( 1 - \frac{(t - t_{0,j})^2}{\Delta_j^2} \right) \quad (4)$$

and

$$f_j(t, t_{0,j}) = 1 - \frac{(t - t_{0,j})^2}{\Delta_j^2}, \quad (5)$$

$\Theta$  being the Heaviside function. The set of parameters  $w_\gamma, \eta, t_0, t_{0,j}, c_j, \Delta_j$  and  $N$  specifies each quench model: for  $\mathcal{A}(2)$ , two overlapping short pulses, the parameters are  $w_\gamma = 0$ ,  $N = 2$ ,  $c_1 = 1$ ,  $\Delta_{1,2} = 1$ ,  $t_{0,1} = \frac{5}{4}\Delta_1$ ,  $c_2 = 2$ ,  $t_{0,2} = \frac{9}{4}\Delta_2$ ; the quench ends at  $t_f^{\mathcal{A}} = 3.25$ . Model  $\mathcal{B}$ , a short pulse superimposed to a slow deformation, is obtained using  $w_\gamma = \frac{2}{5}$ ,  $\eta = 1.2$ ,  $t_0 = 0.25$ ,  $N = 1$ ,  $c_1 = 1$ ,  $\Delta_1 = 1$ ,  $t_{0,1} = 4\Delta_1$ ; the pulse ends at  $t_f^{\mathcal{B}} = 5$ , while a slow distortion continues approaching a constant value. In both models, with profiles  $\gamma(t)$  drawn in the top panels of Fig. 4, the quench starts at  $t_i = 0.25$ . The Einstein equations with quenches have been solved numerically [28], determining the metric functions  $A(r, t)$ ,  $\Sigma(r, t)$  and  $B(r, t)$  that will be used in the analysis of the quarkonium dissociation. Computing the boundary theory stress-energy tensor for the two models, it was found that quantities such as the energy density follow a viscous hydrodynamics behavior immediately after the end of the spikes in the quenches, at  $t_{hydro}^{\mathcal{A}(2)} = 3.25$  and  $t_{hydro}^{\mathcal{B}} = 5$ , while a pressure anisotropy  $\frac{p_\parallel}{p_\perp}$  persists for a longer time, up to  $t_{isotr}^{\mathcal{A}(2)} = 6$  and  $t_{isotr}^{\mathcal{B}} = 6.74$  [28].

To describe a quark-antiquark pair produced in a far-from-equilibrium medium, we consider a classical string in the higher dimensional space described by the metric (2), with endpoints kept close to the boundary. The

---

<sup>2</sup> We denote the proper time as  $t$ , using  $\tau$  for one of the string world-sheet coordinates.

string dynamics is governed by the equations of motion from the Nambu-Goto action

$$S_{NG} = -T_f \int d\tau d\sigma \sqrt{-g} = \int d\tau d\sigma \mathcal{L}_{NG} \quad (6)$$

with  $T_f = \frac{1}{2\pi\alpha'}$ ,  $\alpha' = \frac{L^2}{\sqrt{\lambda}}$ ,  $L$  the AdS<sub>5</sub> radius and  $\lambda$  the 't Hooft coupling.  $g$  is the determinant of the induced world-sheet metric, and  $(\tau, \sigma)$  the world-sheet coordinates. The string profile is described by the embedding functions  $X^M(\tau, \sigma)$ , so that

$$-g = \left[ G_{MN} \dot{X}^M X'^N \right]^2 - (\dot{X})^2 (X')^2, \quad (7)$$

in terms of  $\dot{X}^M = \partial_\tau X^M$  and  $X'^M = \partial_\sigma X^M$ , with  $G_{MN}$  the metric in (2). For strings living in a three-dimensional slice of the dual space described by the coordinates  $(t, w, r)$ , we focus on two possibilities. The first one is  $w = x$ , with  $x = x_1$  or  $x = x_2$  one of the two transverse coordinates, and the string endpoints kept fixed at distance  $2L$  close to the boundary. The second one is  $w = y$  along the rapidity axis, representing a quark and an antiquark moving away from each other in the longitudinal direction  $x_{\parallel}$  with rapidity  $y_L$ .

In the gauge  $\tau = t$  and  $\sigma = w$  the string profile is described by the function  $r(t, w)$ . The Nambu-Goto action can be written in terms of the metric functions in Eq. (2):

$$S_{NG} = -T_f \int dt dw \sqrt{-g} = -T_f \int dt dw \sqrt{\Sigma_w(t, r) (A(t, r) - 2\partial_t r)^2 + (\partial_w r)^2}, \quad (8)$$

where  $\Sigma_w = \bar{\Sigma} = \Sigma^2 e^{-2B}$  if  $w = y$ , and  $\Sigma_w = \tilde{\Sigma} = \Sigma^2 e^B$  if  $w = x$ . Defining  $\mathcal{L}_{NG} = -T_f \sqrt{-g}$  in (8), the canonical momentum densities of the string can be computed,

$$\pi_M^a = \frac{\partial \mathcal{L}_{NG}}{\partial (\partial_a X^M)}, \quad (9)$$

obtaining

$$\begin{pmatrix} \pi_t^0 & \pi_t^1 \\ \pi_w^0 & \pi_w^1 \\ \pi_r^0 & \pi_r^1 \end{pmatrix} = -\frac{T_f}{\sqrt{-g}} \begin{pmatrix} \Sigma_w(A - \dot{r}) + r'^2 & -r'\dot{r} \\ \Sigma_w r' & \Sigma_w(A - 2\dot{r}) \\ -\Sigma_w & r' \end{pmatrix},$$

and the equations of motion

$$\frac{\partial \mathcal{L}_{NG}}{\partial X^M} - \frac{d}{d\tau} \pi_M^0 - \frac{d}{d\sigma} \pi_M^1 = 0. \quad (10)$$

We pause here, before considering the time-dependent geometry, since it is interesting to analyze three simpler cases of a 5D geometry with Eddington-Finkelstein coordinates as in (2), and the dynamics of a string with profile described by a function  $r(t)$  depending only on the time coordinate. The three cases are AdS<sub>5</sub>, AdS<sub>5</sub> with a BH, and AdS<sub>5</sub> with a black-brane, e.g. a BH with time-dependent horizon position as in a hydrodynamic dual. The dissociation time turns out to be finite in our coordinate system.

In pure AdS<sub>5</sub>, described by metric functions  $A(r, t) = \tilde{\Sigma}(r, t) = r^2$  and  $\bar{\Sigma}(r, t) = r^2 t^2$ , the time required for a string to move from an initial position to the AdS center can be easily computed.  $\mathcal{L}_{NG}$  does not depend explicitly on time, and the conjugate momentum  $\pi_t^0$  is a constant of motion, denoted as  $p$ :  $\pi_t^0 = -\frac{\tilde{\Sigma}(A - \dot{r})}{\sqrt{\tilde{\Sigma}(A - 2\dot{r})}} = p$  (we consider the case  $\Sigma_w = \tilde{\Sigma}$ , setting  $T_f = 1$ ). With the initial condition  $r_0 = r(t_i)$  the value of  $r$  at the initial time  $t_i$ , and  $\dot{r}(t_i) = \dot{r}_0$ , one has

$$\dot{r} = \frac{r^4 - p(p - \sqrt{p^2 - r^4})}{r^2}, \quad (11)$$

$$p = -\frac{r_0(r_0^2 - \dot{r}_0)}{\sqrt{r_0^2 - 2\dot{r}_0}}. \quad (12)$$

Starting from  $r_0$ , the position  $r$  is reached after the time lapse

$$\Delta t = t - t_i = \int_{r_0}^r dr \frac{1}{\dot{r}} \quad (13)$$

that can be computed analytically:

$$\Delta t^{AdS} = \frac{1}{r_0 x} \left\{ \frac{x}{1 - v_0} - 1 + \sqrt{1 - x^4 q^4} - x q \left[ E(\text{ArcSin}(q), -1) - E(\text{ArcSin}(qx), -1) - F(\text{ArcSin}(q), -1) + F(\text{ArcSin}(qx), -1) \right] \right\}, \quad (14)$$

with  $x = \frac{r}{r_0}$ ,  $v_0 = \frac{\dot{r}_0}{r_0^2}$ ,  $q = \frac{(1 - 2v_0)^{1/4}}{(1 - v_0)^{1/2}}$ .  $F$  and  $E$  are elliptic integrals of the first and second kind, respectively. For  $\dot{r}_0 = 0$  the result is:

$$\Delta t^{AdS} = \frac{1}{r_0 x} \left\{ -1 + \sqrt{1 - x^4} + x \left[ 1 - E(-1) + E(\text{ArcSin}(x), -1) - F(\text{ArcSin}(x), -1) + K(-1) \right] \right\}, \quad (15)$$

the function  $E$  with a single argument being the complete elliptic integral of the second kind, and  $K$  the complete elliptic integral of the first kind. Equation (15) implicitly defines the string profile  $r(t)$ . The AdS center is reached in a finite time lapse, since for  $r \rightarrow 0$

$$t_D^{AdS} = t - t_i = \frac{1}{r_0} \left( 1 - \frac{\sqrt{2}\pi^{3/2}}{\Gamma(\frac{1}{4})^2} \right). \quad (16)$$

In AdS black-hole geometry described by the metric functions

$$A(r, t) = r^2 \left( 1 - \frac{r_H^4}{r^4} \right), \quad \tilde{\Sigma}(r, t) = r^2, \quad \bar{\Sigma}(r, t) = r^2 t^2, \quad (17)$$

the time interval  $\Delta t$  can also be analytically determined for a generic  $\dot{r}_0$ . For  $\dot{r}_0 = 0$  one has

$$\dot{r} = - \frac{r_0^4 - r^4 + \sqrt{(r_0^4 - r^4)(r_0^4 - r_H^4)}}{r^2}. \quad (18)$$

Using  $Y = \sqrt{1 - \frac{r_H^4}{r_0^4}}$  and  $P = \sqrt{1 - \frac{r^4}{r_0^4}}$ , the time to reach the position  $r$  starting from  $r = r_0$  is

$$\Delta t^{BH} = \frac{2\sqrt{2}}{3r_0(1+Y)} \left[ F_1\left(\frac{3}{4}, \frac{1}{2}, 1, \frac{7}{4}, -1, \frac{1-Y}{1+Y}\right) - \frac{(1-P^2)^{\frac{3}{4}}}{(1+P)^{\frac{3}{2}}} F_1\left(\frac{3}{4}, \frac{1}{2}, 1, \frac{7}{4}, -\frac{1-P}{1+P}, \frac{1-P}{1+P} \frac{1-Y}{1+Y}\right) \right], \quad (19)$$

with  $F_1$  the Appell hypergeometric function of two variables. Also Eq. (19) implicitly defines the string profile  $r(t)$ . The time required to reach the horizon  $r = r_H$  is obtained substituting  $P \rightarrow Y$ :

$$t_D^{BH} = t - t_i = \frac{2\sqrt{2}}{3r_0(1+Y)^{7/4}} \left[ (1+Y)^{\frac{3}{4}} F_1\left(\frac{3}{4}, \frac{1}{2}, 1, \frac{7}{4}, -1, \frac{1-Y}{1+Y}\right) - (1-Y)^{\frac{3}{4}} F_1\left(\frac{3}{4}, \frac{1}{2}, 1, \frac{7}{4}, -\frac{1-Y}{1+Y}, \frac{(1-Y)^2}{(1+Y)^2}\right) \right]. \quad (20)$$

For  $Y \rightarrow 0$  we recover Eq. (16) for pure AdS<sub>5</sub>.

The result for the black-brane geometry with time-dependent horizon can be obtained from the previous one, considering  $r_H = r_H(t)$ . The geometry dual to viscous hydrodynamics derived in [30] belongs to this class of geometries. If in the interval  $\Delta t$  the change in horizon position is small, the string profile can still be found substituting  $r_H \rightarrow r_H(t)$  in Eq. (19):

$$\Delta t^{HYDRO} = t - t_i = \frac{2\sqrt{2}}{3r_0(1+Y(t))} \left[ F_1\left(\frac{3}{4}, \frac{1}{2}, 1, \frac{7}{4}, -1, \frac{1-Y(t)}{1+Y(t)}\right) - \frac{(1-P^2)^{\frac{3}{4}}}{(1+P)^{\frac{3}{2}}} F_1\left(\frac{3}{4}, \frac{1}{2}, 1, \frac{7}{4}, -\frac{1-P}{1+P}, \frac{1-P}{1+P} \frac{1-Y(t)}{1+Y(t)}\right) \right] \quad (21)$$

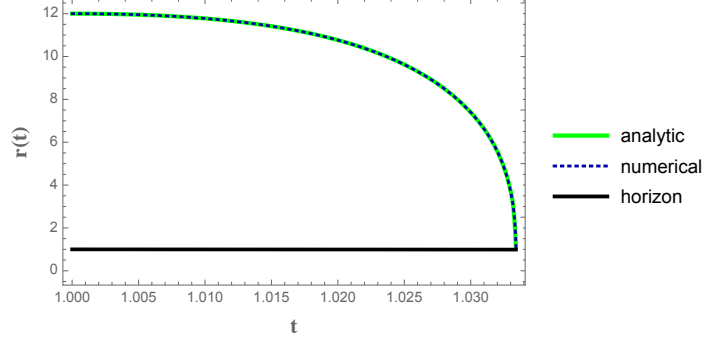


FIG. 1. String profile  $r(t)$  for the AdS-BH and  $t$ -dependent horizon (25), obtained using the expressions in (21),(22) and the numerical solution of (23) (with  $r_0 = 12$ ,  $t_i = 1$  and  $e_0 = 3$ ).

with

$$Y(t) = \sqrt{1 - \frac{r_H(t)^4}{r_0^4}}. \quad (22)$$

Equation (21) implicitly defines the string profile  $r(t)$  which solves Eq. (10) for  $M = 5$  and AdS-BH metric functions with time-dependent  $r_H(t)$ :

$$r(t)^2 \ddot{r}(t) - 6r(t)^3 \dot{r}(t) - 2r(t)(r_H(t)^4 - \dot{r}(t)^2) + 2r(t)^5 + 2r_H(t)^3 \dot{r}_H(t) = 0. \quad (23)$$

This can be shown dividing the interval  $[t_i, t_D]$  of (23) in equal-size intervals of infinitesimal width,  $[t_i, t_D] = \bigcup_{k=1}^N [t_k, t_{k+1}]$ , where  $t_{k+1} - t_k = \epsilon$ ,  $t_0 = t_i$ ,  $t_{N+1} = t_D$ , and  $\epsilon \rightarrow 0$ ,  $N \rightarrow \infty$ . In each time interval, we solve (23) with the substitution  $r_H(t) = r_H(t_k) = r_H(t_{k+1})$ , provided that the  $r_H(t)$  changes with time slower than the solution  $r(t)$ , obtaining that Eq. (23) coincides with the corresponding one for a static AdS-BH geometry,

$$r(t)^2 \ddot{r}(t) - 6r(t)^3 \dot{r}(t) - 2r(t)(r_H(t_k) - \dot{r}(t)^2) + 2r(t)^5 = 0. \quad (24)$$

The implicit solution of (24) is given by Eq. (19), which solves (23) in  $[t_k, t_{k+1}]$ . Considering all intervals and taking  $N \rightarrow \infty$ , one finds that Eq. (19) provides the solution for the black-brane characterized by the horizon  $r_H(t)$ .

The time  $t_H$  at which the horizon is reached can be computed solving numerically the equation  $t_H - t_i = \Delta t^{HYDRO}$ , with  $r(t_H) = r_H(t_H)$ . To check that Eq. (21) provides the solution of (24), we choose, e.g.,

$$r_H(t) = \left(\frac{e_0}{3}\right)^{1/4} \frac{1}{t^{1/3}}, \quad (25)$$

corresponding to inviscid hydrodynamics [30], we fix  $t_i = 1$  and  $e_0 = 3$  and solve numerically (24). The solution coincides with Eq. (21) as shown in Fig. 1. At odds with the static cases (14) and (19), the explicit  $t$ -dependence in (21) induces a nontrivial relation between  $t_D$  and  $t_i$ , as we shall see in the following.

An approximate large- $t$  solution for the string profile in an AdS black-brane metric with time-dependent horizon is  $r(t) \sim \frac{1}{t^{1/3}}$ , as it can be verified plugging this function in (23) and observing that the equation is satisfied but for terms  $\mathcal{O}(t^{-7/3})$ .<sup>3</sup> This allows to compute the asymptotic (large- $t$ ) value of the dissociation time  $t_D$ ,

$$t_\infty = \frac{2}{3r_0} {}_2F_1\left(1, \frac{5}{4}, \frac{7}{4}, -1\right) \quad (26)$$

<sup>3</sup> A similar behavior is found for large  $t$  in the Fefferman-Graham coordinates [24].

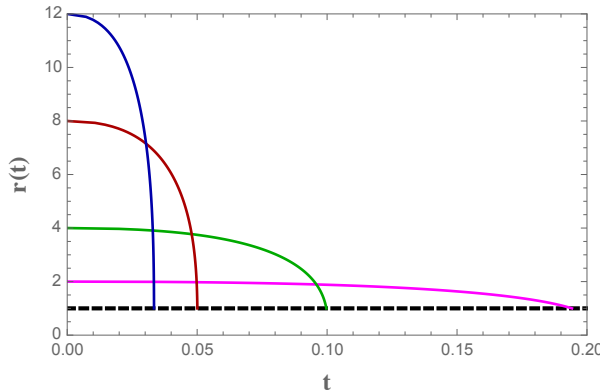


FIG. 2. String profile  $r(t)$  in the AdS-BH metric (17) and transverse  $w = x$  configuration, for  $r_0 = 12$  (blue line),  $r_0 = 8$  (red),  $r_0 = 4$  (green) and  $r_0 = 2$  (pink).

which coincides with (16). For  $r_0 = 12$ , an input value in our analysis,  $t_\infty = 0.0334108$  is obtained. As it will be shown in Fig. 8, this value is rapidly approached by the dissociation time  $t_D$  computed with the metric functions  $A$ ,  $\Sigma$  and  $B$  of the geometry with quenches.

A feature of the solution is that  $t_D$  decreases when the starting point  $r_0$  is closer to the boundary, as shown in Fig. 2 for the AdS-BH with  $r_H = 1$ . Identifying the position of the string endpoints near the boundary with the quark mass [13], this implies that a heavier quarkonium dissociates faster than a lighter one.

Let us now consider the metric functions for the out-of-equilibrium system [28]. They are characterized by two regimes. In the early-time regime the geometry abruptly responds to the external quenches, a black-hole is formed with a rapidly changing horizon position [26, 27]. After the pulses are switched off, a black-brane geometry is recovered, with the metric functions reconstructed in [29]. The horizon position is found with time dependence

$$r_H(t) = \frac{\pi\Lambda}{(\Lambda t)^{1/3}} \left[ 1 - \frac{1}{6\pi(\Lambda t)^{2/3}} + \frac{-1 + \log 2}{36\pi^2(\Lambda t)^{4/3}} + \frac{-21 + 2\pi^2 + 51 \log 2 - 24(\log 2)^2}{1944\pi^3(\Lambda t)^2} + \mathcal{O}\left(\frac{1}{(\Lambda t)^{8/3}}\right) \right]. \quad (27)$$

The parameters  $\Lambda^{\mathcal{B}} = 1.12$  and  $\Lambda^{\mathcal{A}(2)} = 1.73$  refer to the two quench model. Equation (25) is the leading term of (27). The late-time regime is dual to viscous hydrodynamics.

The equation for the string profile  $r(t, w)$  obtained from Eqs.(8) and (10) and  $M = 5$  reads:

$$r'' - \frac{\partial_w g}{2g} r' + \frac{\partial_t g}{2g} \Sigma_w - \partial_t \Sigma_w + \frac{\partial_r g}{2} = 0. \quad (28)$$

Choosing  $w = y$  or  $w = x$ , the equations can be solved imposing suitable boundary and initial conditions. In our time-dependent metric we vary the initial time  $t_i$  at which to start considering the string evolution. At  $t_i$  the string is completely stretched close to the boundary,  $r(t_i, w) = r_{max}$  for all  $w$ , with  $r_{max}$  the maximum value of the radial coordinate used in the numerical calculation ( $r_{max} = 12$ ). The string endpoints are kept fixed at  $w_Q = -L$  and  $w_{\bar{Q}} = L$  for the transverse configuration, and  $w_Q = -y_L$  and  $w_{\bar{Q}} = y_L$  for the  $w = y$  configuration, so that  $r(t, w_{\bar{Q}}) = r(t, w_Q) = r_{max}$  for all  $t$ . We study the dependence on the spatial and rapidity separation varying  $L$  and  $y_L$  in the range  $[0.1, 100]$ . As a further condition, we impose  $\dot{r}(t_i, w) = v$ , with  $v = 0, -0.5, -1$ .

In Fig. 3 we show the string profile in the quench model  $\mathcal{B}$ , in the case  $w = x$  and separation  $L = 0.1$ . Similar results are found for the  $w = y$  configuration and for model  $\mathcal{A}(2)$ . The dissociation time  $t_D$  is obtained when the horizon is reached.

The dependence of  $t_D$  on the starting time  $t_i$  is depicted in Fig. 4 for the two models. In each column we draw the quench profile (upper panel) and  $t_D$  for the longitudinal  $w = y$  configuration with  $y_L = 10$  (middle panel), and transverse  $w = x$  configuration with  $L = 10$  (bottom panel). In both models the dissociation times exhibit abrupt fluctuations during the quenches, with a tiny delay from the maxima of the pulses. Soon after the end of the quenches,  $t_D$  varies smoothly and approaches the same value in both models. During the

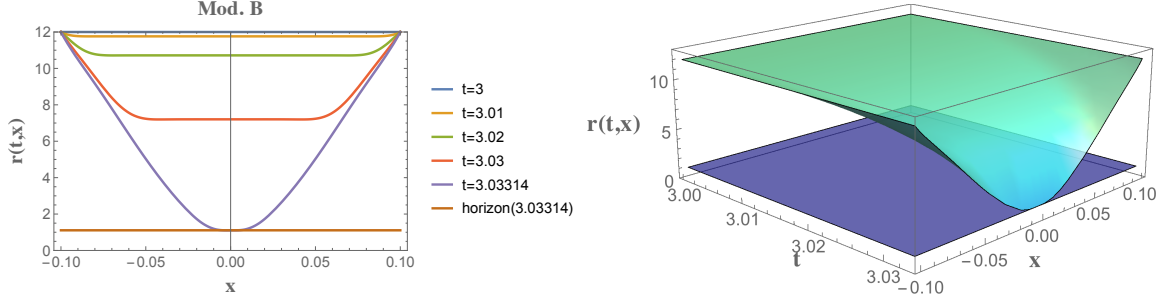


FIG. 3. String profile  $r(t, w)$ , corresponding to  $\{t_i, v, L\} = \{3, -1, 0.1\}$ , for the transverse  $w = x$  configuration and quench model  $\mathcal{B}$ . Left: profile as a function of  $x$  at different  $t$ , until the horizon is reached. Right: solution  $r(t, x)$  (sea-green surface). The blue surface corresponds to the horizon.

quenches, the behavior of  $t_D$  is different for the longitudinal and transverse string configurations, the maxima correspond to minima when switching from one configuration to the other. This is reminiscent of the behavior of the longitudinal  $p_{\parallel}$  and transverse  $p_{\perp}$  pressure [28], maxima in  $p_{\parallel}$  correspond to minima in  $p_{\perp}$  and viceversa.

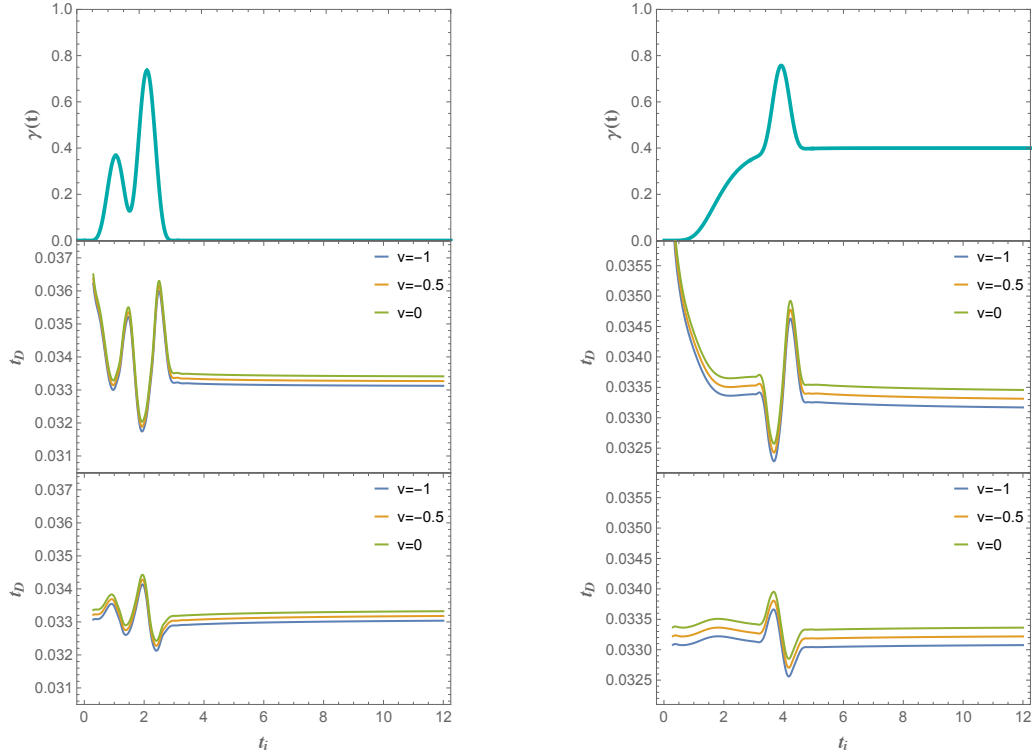


FIG. 4. Quarkonium dissociation time  $t_D$  versus  $t_i$  in quench model  $\mathcal{A}(2)$  (left) and  $\mathcal{B}$  (right). The quench profiles  $\gamma(t)$  are drawn in the top panels. The middle plots refer to the  $w = y$  string configuration with  $y_L = 10$ , the bottom plots to the transverse  $w = x$  configuration and  $L = 10$ . Results are shown for three values of the initial velocity  $v$ , indicated in the legends.

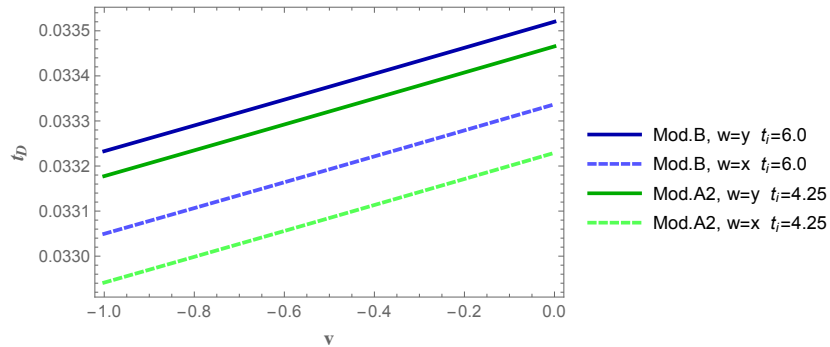


FIG. 5. Dissociation time  $t_D$  versus  $v$  for models  $\mathcal{A}(2)$  and  $\mathcal{B}$ , in the transverse  $w = x$  configuration with separation  $L = 10$  and in the  $w = y$  configuration with  $y_L = 10$ . The initial time is chosen in such a way that the same  $\Delta t = 1$  has elapsed after the end of the quench for each model.

However, a connection between the two sets of observables justifying the analogous behavior of pressures and dissociation times is difficult to establish.

Dissociation is faster for  $w = x$ , with the string in a plane transverse to the collision axis. This is in agreement with the results of several studies suggesting that the orientation of the string and the position of its endpoints are relevant for the dual field interpretation of the quarkonium properties. For example, in Ref. [20] it has been found that the direction of the string with respect to the hot wind, namely to the velocity of the fluid produced in the collision, affects the quarkonium screening length, which is minimum for a string oriented perpendicular to the wind and maximum for one parallel to it. Such a pattern is consistent with our results for the dissociation time, since the cases  $w = y$  and  $w = x$  correspond, respectively, to a quark-antiquark pair parallel and perpendicular to the direction along which the plasma expands. Other results with similar interpretation are reported in [31, 32].

We also observe a mild dependence on the initial velocities: varying  $v$  in the range  $[-1, 0]$ , a linear dependence of  $t_D$  is found for both the quench models and string configurations, as shown in Fig. 5 where the initial time is fixed in such a way that the same  $\Delta t = 1$  has elapsed after the end of the boundary metric distortion. The linear  $v$  dependence is expressed in terms of the intercept  $a^{M,w}$  and slope  $b^{M,w}$ , for the two models  $M = \mathcal{B}, \mathcal{A}(2)$  and configurations  $w = x, y$ :  $a^{\mathcal{B},x} = 0.0333366$  and  $b^{\mathcal{B},x} = 0.000287307$ ,  $a^{\mathcal{B},y} = 0.0335199$  and  $b^{\mathcal{B},y} = 0.000287263$ ,  $a^{\mathcal{A}(2),x} = 0.0332289$  and  $b^{\mathcal{A}(2),x} = 0.000287869$ ,  $a^{\mathcal{A}(2),y} = 0.0334651$  and  $b^{\mathcal{A}(2),y} = 0.00028788$ . The slopes are compatible with the result of Eq. (14).

Varying the separation between the string endpoints, we obtain the results in Figs. 6 and 7 for the different models and configurations and for selected initial time. Three values of  $t_i$  in Fig. 7 correspond to the start of the first pulse, the peak and the end of the last pulse, and three values are taken after the last pulse is switched off. Our algorithm is able to determine the dissociation times up to small values of the separation,  $L = 0.1$  and  $y_L = 0.1$ .  $t_D$  remains largely independent of the separation, with some fluctuations ascribed in part to numerical effects that can be reduced using a method of changing variables proposed in [24].

Dissociation is a fast phenomenon. It is strongly affected by the quenches and, as in systems with nonlinearities, it does not closely follow the quench profiles. Similarly to some local observables, namely the energy density, as soon as the last pulse is switched off the behavior in the geometry dual to viscous hydrodynamics is recovered, as it can be seen in Fig. 8. The figure also shows that, although the hydrodynamic model could provide a description of the late time behavior ( $t > 6$  in model  $\mathcal{B}$ ), it is not able to capture the properties of the system during the rapidly varying regime. Setting the physical units as in [28], assuming a temperature of the system after the quenches  $T \sim 500$  MeV, the dissociation time is  $\mathcal{O}(10^{-2})$  fm.

An interesting issue to comment on is that, as observed in [26] and [33], in the approach of boundary sourcing the boundary metric is flat in the  $t = \pm\infty$  limit and is curved in correspondence of the pulses, so that is worth asking if the effect of the curved boundary can be separated from the genuine out-of-equilibrium effect in determining the dissociation times. Although such a separation is difficult to implement analytically, one can observe that for both the considered quench models the time profiles of the boundary curvature invariants (Ricci and Kretschmann scalars) are different from the dissociation time profiles displayed in Fig. 4. Moreover, we found that  $t_D$  depends on the string orientation in correspondence of the pulses. This difference in time profiles induces us to argue that the genuine out-of-equilibrium matter effect is captured in correspondence of



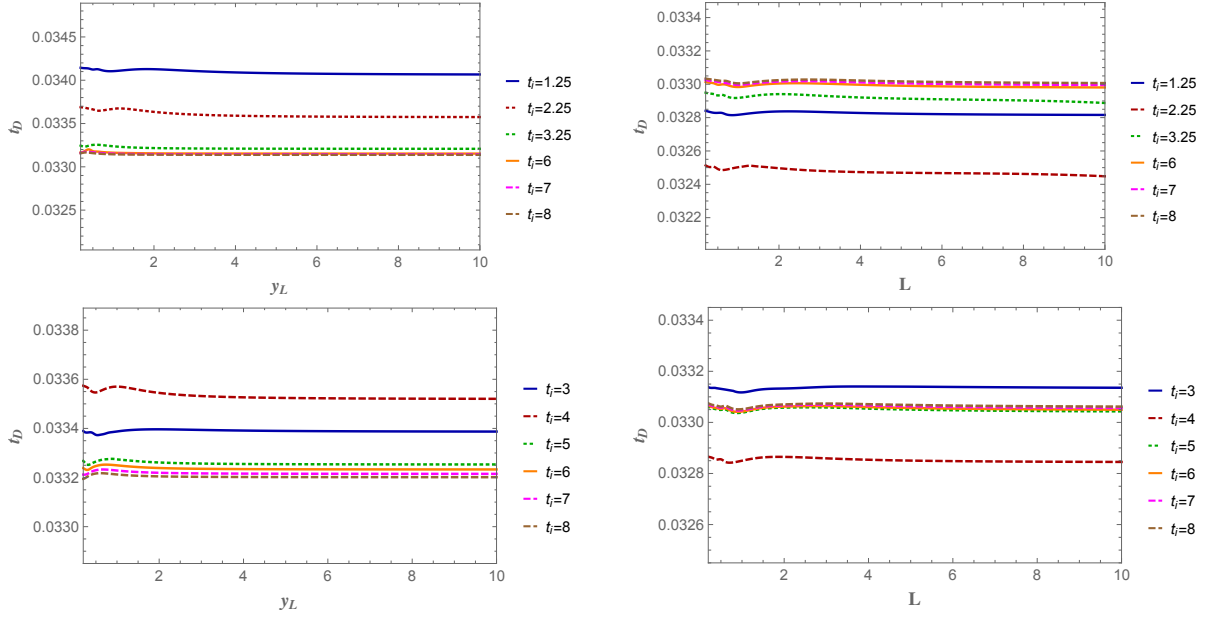


FIG. 6. Dissociation time  $t_D$  for several values of the initial time, for quench model  $\mathcal{A}(2)$  (upper plots) and  $\mathcal{B}$  (lower plots), and initial velocity  $v = -1$ . Left:  $t_D$  versus rapidity separation  $y_L$  for the  $w = y$  string configurations. Right:  $t_D$  versus separation  $L$  for the transverse  $w = x$  configuration.

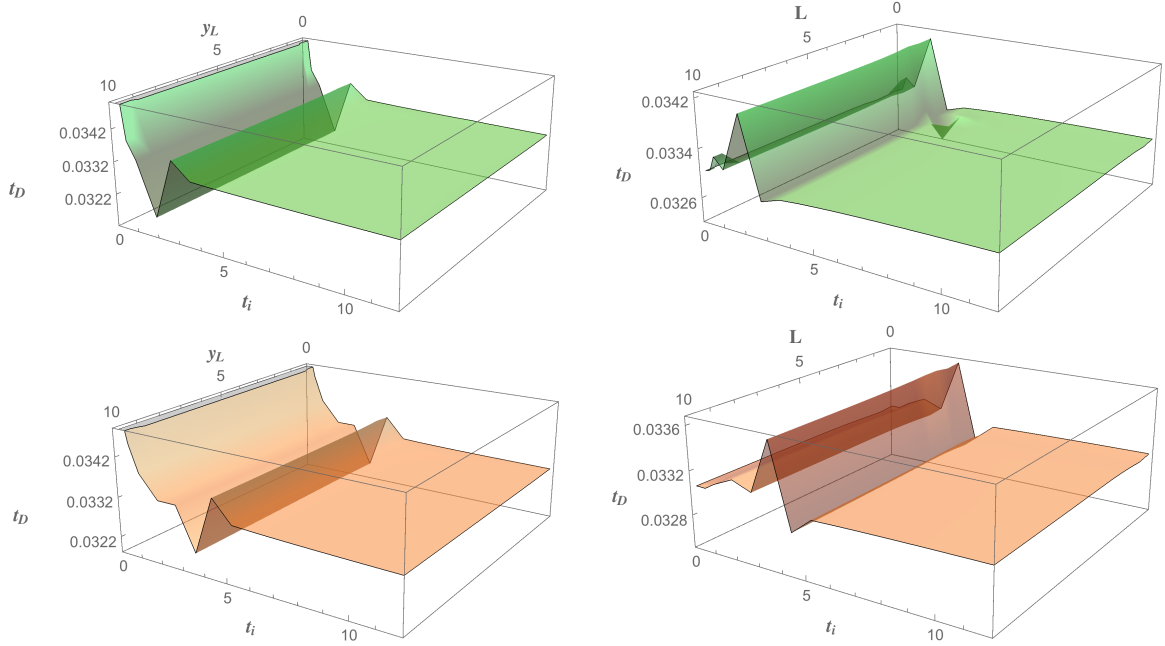


FIG. 7. Quarkonium dissociation time  $t_D$  for quench model  $\mathcal{A}(2)$  (upper plots) and  $\mathcal{B}$  (lower plots) and initial velocity  $v = -1$ . Left:  $t_D$  vs  $t_i$  and rapidity separation  $y_L$  for the configuration  $w = y$ . Right:  $t_D$  vs  $t_i$  and separation  $L$  for the transverse  $w = x$  configuration.

the boundary pulses.

Before concluding our study of the real-time quarkonium dissociation dynamics in a far-from-equilibrium

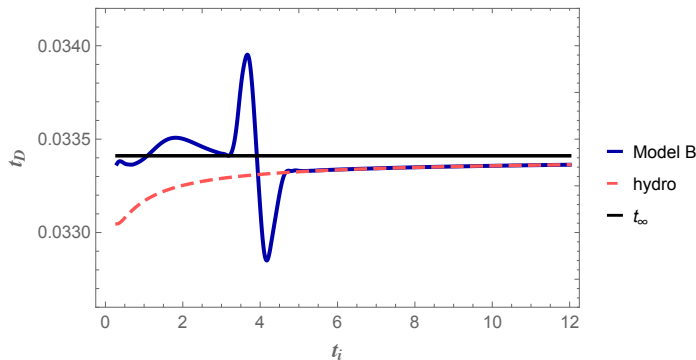


FIG. 8. Quarkonium dissociation time  $t_D$  versus  $t_i$  for the transverse configuration  $w = x$ , with separation  $L = 10$  and  $v = 0$ . The continuous line is the result for quench model  $\mathcal{B}$ , the dashed line for a geometry dual to viscous hydrodynamics, with horizon  $r_H(t)$  in (27). The horizontal line corresponds to the asymptotic value in Eq. (26).

plasma, we remark that in our models the confinement effects are not accounted for. In the holographic framework, a mechanism producing confinement in a strongly-coupled system can be implemented by a self-interacting scalar field dual to a relevant deformation of the boundary conformal field theory [34], with a scalar potential designed to produce expected features of QCD, a crossover, a 1st or a 2nd order deconfinement transition [35–37]. In the critical regions of the QCD phase diagram the role of nonhydrodynamical degrees of freedom seems more pronounced than in models similar to the one we have considered [37]. The description of the real-time quarkonium evolution in such models, driven out-of-equilibrium, and the comparison with the results obtained here deserve dedicated analyses.

### Acknowledgments

This study has been carried out within the INFN project (Iniziativa Specifica) QFT-HEP.

- 
- [1] P. Braun-Munzinger, V. Koch, T. Schfer, and J. Stachel, Phys. Rept. **621**, 76 (2016), arXiv:1510.00442 [nucl-th].
  - [2] J. Schukraft, arXiv:1705.02646 [hep-ex].
  - [3] P. Romatschke, Eur. Phys. J. **C77**, 21 (2017), arXiv:1609.02820 [nucl-th].
  - [4] T. Matsui and H. Satz, Phys. Lett. **B178**, 416 (1986).
  - [5] J. M. Maldacena, Int.J.Theor.Phys. **38**, 1113 (1999), arXiv:hep-th/9711200 [hep-th].
  - [6] E. Witten, Adv.Theor.Math.Phys. **2**, 253 (1998), arXiv:hep-th/9802150 [hep-th].
  - [7] S. Gubser, I. R. Klebanov, and A. M. Polyakov, Phys.Lett. **B428**, 105 (1998), arXiv:hep-th/9802109 [hep-th].
  - [8] M. Ammon and J. Erdmenger, *Gauge/gravity duality* (Cambridge Univ. Pr., Cambridge, UK, 2015).
  - [9] P. M. Chesler and L. G. Yaffe, JHEP **07**, 086 (2014), arXiv:1309.1439 [hep-th].
  - [10] J. Casalderrey-Solana, H. Liu, D. Mateos, K. Rajagopal, and U. A. Wiedemann, (2011), arXiv:1101.0618 [hep-th].
  - [11] A. Karch and E. Katz, JHEP **06**, 043 (2002), arXiv:hep-th/0205236 [hep-th].
  - [12] S. S. Gubser, Phys. Rev. **D74**, 126005 (2006), arXiv:hep-th/0605182 [hep-th].
  - [13] C. P. Herzog, A. Karch, P. Kovtun, C. Kozcaz, and L. G. Yaffe, JHEP **07**, 013 (2006), arXiv:hep-th/0605158 [hep-th].
  - [14] J. Casalderrey-Solana and D. Teaney, Phys. Rev. **D74**, 085012 (2006), arXiv:hep-ph/0605199 [hep-ph].
  - [15] M. Chernoicoff, J. A. Garcia, and A. Guijosa, JHEP **09**, 068 (2006), arXiv:hep-th/0607089 [hep-th].
  - [16] P. M. Chesler and K. Rajagopal, Phys. Rev. **D90**, 025033 (2014), arXiv:1402.6756 [hep-th].
  - [17] P. M. Chesler, K. Jensen, and A. Karch, Phys. Rev. **D79**, 025021 (2009), arXiv:0804.3110 [hep-th].
  - [18] P. M. Chesler, K. Jensen, A. Karch, and L. G. Yaffe, Phys. Rev. **D79**, 125015 (2009), arXiv:0810.1985 [hep-th].
  - [19] S. S. Gubser, D. R. Gulotta, S. S. Pufu, and F. D. Rocha, JHEP **10**, 052 (2008), arXiv:0803.1470 [hep-th].
  - [20] H. Liu, K. Rajagopal, and U. A. Wiedemann, Phys. Rev. Lett. **98**, 182301 (2007), arXiv:hep-ph/0607062 [hep-ph].
  - [21] H. Liu, K. Rajagopal, and U. A. Wiedemann, JHEP **03**, 066 (2007), arXiv:hep-ph/0612168 [hep-ph].
  - [22] S. I. Finazzo and J. Noronha, JHEP **01**, 051 (2015), arXiv:1406.2683 [hep-th].
  - [23] M. Ali-Akbari, F. Charmchi, A. Davody, H. Ebrahim, and L. Shahkarami, Phys. Rev. **D93**, 086005 (2016), arXiv:1510.00212 [hep-th].
  - [24] S. Lin and E. Shuryak, Phys. Rev. **D77**, 085013 (2008), arXiv:hep-ph/0610168 [hep-ph].

- [25] I. Iatrakis and D. E. Kharzeev, Phys. Rev. **D93**, 086009 (2016), arXiv:1509.08286 [hep-ph].
- [26] P. M. Chesler and L. G. Yaffe, Phys. Rev. Lett. **102**, 211601 (2009), arXiv:0812.2053 [hep-th].
- [27] P. M. Chesler and L. G. Yaffe, Phys. Rev. **D82**, 026006 (2010), arXiv:0906.4426 [hep-th].
- [28] L. Bellantuono, P. Colangelo, F. De Fazio, and F. Giannuzzi, JHEP **07**, 053 (2015), arXiv:1503.01977 [hep-ph].
- [29] L. Bellantuono, P. Colangelo, F. De Fazio, F. Giannuzzi, and S. Nicotri, Phys. Rev. **D94**, 025005 (2016), arXiv:1603.08849 [hep-ph].
- [30] R. A. Janik and R. B. Peschanski, Phys. Rev. **D73**, 045013 (2006), arXiv:hep-th/0512162 [hep-th].
- [31] M. Natsuume and T. Okamura, JHEP **09**, 039 (2007), arXiv:0706.0086 [hep-th].
- [32] K. Bitaghsir Fadafan and S. K. Tabatabaei, Phys. Rev. **D94**, 026007 (2016), arXiv:1512.08254 [hep-ph].
- [33] L. Keegan, A. Kurkela, P. Romatschke, W. van der Schee, and Y. Zhu, JHEP **04**, 031 (2016), arXiv:1512.05347 [hep-th].
- [34] S. S. Gubser, A. Nellore, S. S. Pufu, and F. D. Rocha, Phys. Rev. Lett. **101**, 131601 (2008), arXiv:0804.1950 [hep-th].
- [35] T. Ishii, E. Kiritsis, and C. Rosen, JHEP **08**, 008 (2015), arXiv:1503.07766 [hep-th].
- [36] R. A. Janik, J. Jankowski, and H. Soltanpanahi, JHEP **06**, 047 (2016), arXiv:1603.05950 [hep-th].
- [37] R. A. Janik, J. Jankowski, and H. Soltanpanahi, Phys. Rev. Lett. **117**, 091603 (2016), arXiv:1512.06871 [hep-th].